JOURNAL OF AIRCRAFT
Vol. 44, No. 2, March–April 2007

Finite Element Modeling of a Bird Striking an Engine Fan Blade

R. H. Mao,* S. A. Meguid,† and T. Y. Ng‡
Nanyang Technological University, Singapore 639798, Republic of Singapore

DOI: 10.2514/1.24568

Bird strike is a serious problem that affects both commercial and military aircrafts. Systematic modeling and simulation of bird strikes are severely lacking, especially for cases involving engine, fan blades, and casings. In the present investigation, explicit 3-D finite element analysis using LS-DYNA is carried out to study the nonlinear transient response of a bird striking a fan system. The bird strike is simulated using Lagrangian blade–bird formulations. The bird is modeled as a fluid jet with a homogenized fluidic constitutive relation, using the Brockman hydrodynamic model, which was found to be the most appropriate. The present simulations are validated using a benchmark test of a bird striking a rigid target that is reported in the literature. Following this validation, a reference case of a bird striking a flexible fan blade was set up and used as the reference case in a series of parametric studies. The effect of bird velocity and its size are examined and attention is given to strikes involving larger birds so as to address the lack of data in this area.

Nomenclature

D	=	diameter of bird, m
E	=	Young's modulus, Pa
$\dot{e}_{ij}$	=	strain rate tensor, s^{-1}
F	=	impacting force, N
$F_{\max}$	=	maximum impacting force, N
I	=	impulse, $\int_0^t F(\tau)\,d\tau$, N · s
I_{ad}	=	normalized impulse, $I/m\dot{w}_0$
L	=	length of bird, m
m	=	mass of bird, kg
P	=	pressure, Pa
P_{ad}	=	normalized pressure, P/P_s^{TH}
P_s^{TH}	=	theoretical stagnation pressure, $\frac{1}{2}\rho_0\dot{w}_0^2$
T	=	normalized time, $t/(L/\dot{w}_0)$
t	=	time, s
u, v, w	=	displacements in x-, y-, and z-directions, m
$\dot{u}, \dot{v}, \dot{w}$	=	velocities in x-, y-, and z-directions, m/s
$\ddot{u}, \ddot{v}, \ddot{w}$	=	accelerations in x-, y-, and z-directions, m/s^2
$\dot{w}_0$	=	initial velocity of bird, m/s
X, Y, Z	=	Cartesian coordinates, m
γ	=	kinematic viscosity coefficient, m^2/s
ε_e	=	elastic strain
ε_p	=	von Mises plastic strain
$\varepsilon_{p,\max}$	=	maximum plastic strain
μ	=	mass density changing ratio of bird, $\rho/\rho_0 - 1$
ν	=	Poisson ratio
ρ	=	mass density of bird, kg/m^3
ρ_0	=	initial mass density of bird, kg/m^3
σ_{ij}	=	stress tensor, Pa
σ_y	=	yield stress, Pa

Received 13 April 2006; accepted for publication 9 October 2006.

*Post-Doctoral Fellow, Division of Aerospace Engineering, School of Mechanical and Aerospace Engineering.

†Professor and Head, Division of Aerospace Engineering, School of Mechanical and Aerospace Engineering; mshaker@ntu.edu.sg (corresponding author).

‡Associate Professor, Division of Aerospace Engineering, School of Mechanical and Aerospace Engineering.

I. Introduction

FAA statistical data reveal that gas turbine engines are the most vulnerable to bird strikes. In reality, almost all severe accidents are closely related to the failure of the engines, which are the sole suppliers of thrust and power to the entire aircraft. Thus, it is obvious that the problem of a bird striking a fan blade system requires careful investigation. In the 1970s, predominantly experimental techniques were used for evaluating the mechanical integrity and fail-safe resistance of aircraft engine parts subjected to bird strike and ingestion [1]. Barber et al. [2] found that the loads produced by the bird strike were adequately duplicated by representing the bird as a circular cylinder with the same mass, density, and compressibility as the bird. Wilbeck [3] showed that the stresses generated during a high-speed impact greatly exceed the tissue strength of the bird, and that the bird actually behaved like a fluid with negligible viscosity. The hydrodynamic behavior of the impactor projectile is accepted by other researchers, such as Reddy [4], who neglected the strength effect of the solid in the case of hypervelocity impact. A few years later, artificial bird models began to substitute real birds [5]. Today, artificial birds are usually made from gelatin and have been widely adopted by many aerospace companies [6].

With the development of advanced numerical techniques and computing technology, Aiello et al. [7] numerically studied the mechanical performances of hollow blades with composite inlays. They reported that these configurations would improve the crashworthiness of shroudless hollow fan blades. The centrifugal stiffening effect was also found to be beneficial in reducing blade deformation under bird strike through the preliminary dynamic analyses of Shioya and Stronge [8] and Schuette [9]. Miyachi et al. [10] further established that the centrifugal force effect on local deformation is smaller than that on the global scale. Furthermore, the mechanical properties of the blade were determined to be critical to assessing the strike force [11]. Yu and Jones [12] recommended that for impact studies, a complete set of reliable experimental data, including both the structure response and the dynamic properties of the material, would be required for large inelastic analysis. Subsequently, Schuette [9] and Martin [13] proved that the bird properties at high-speed impact scenarios were key parameters as well. The explicit numerical studies of Schuette [9] and Martin [13] concerning a bird striking fan blades revealed that the bird actually behaved like compressible nonlinear fluid, and this was further verified by high-speed photography studies [14,15]. It should be noted, however, that it was only in the late 1980s that the explicit time integration scheme was developed and applied to carry out large deformation simulations, such as bird strike problem. One of these works emerged from Rolls-Royce [16], where the large wide chord

fan blade was tested for its aerodynamic performance. With the help of commercial explicit integration software incorporated with contact-impact algorithm, the bird's slicing effect by the blades was simulated, and achieved good agreements with their respective experimental tests [17–20].

A bird strike is characterized by loads with high intensity and short duration. The exposed target material undergoes high strain rates, large deformations, and inelastic strains. In addition, a greater interaction exists between the impact loads and the response of the structure. Thus, it was only in the late 1980s, with the development of explicit finite element codes, that it became possible to numerically analyze this kind of event with a certain degree of accuracy. The unique difficulties of bird strike simulations include 1) the method adopted in modeling the bird, 2) the geometric intricacy of the bird and the target, 3) the constitutive behavior of the bird and target materials at high impinging speeds, and 4) the type of contact algorithm used.

It has long been noted that the finite element method (FEM) is very powerful in the numerical simulation of the crashworthiness and failure analyses [21], and is more accurate than the finite difference method (FDM) for hypervelocity impact analysis [4]. Canonical Lagrangian formulations, when applied to the bird model, will result in two difficulties: namely, reducing the time step and resulting in adversely distorted elements. When solving dynamic transient nonlinear problems, the time step Δt is closely related to the physical length scale of the smallest element $l_{\min}$ within the model, i.e.,

$$\Delta t = \frac{l_{\min}}{c} \tag{1}$$

where c is the sonic speed in the local medium. For soft-bodied birds, large strain distortions will develop during high-speed impingement. The resulting excessively compressed meshes might decrease the time step to impractical lower values such that the analysis may take unacceptable excessive time. Another difficulty is that elemental volume may become negative, thus producing negative stiffness matrix leading to failure of the analysis. To address these problems, a numerical elimination procedure for elements reaching either the maximum failure strain or the minimum reference value of the time step has been developed and employed by many researchers [22–26]. A typical problem arising from element deletion is the artificial oscillations in the contact forces due to the discretized nature of the simulated contact algorithms, especially for coarse meshes. Once the frontal elements are deleted, the contact force will decrease dramatically until the impactor comes into contact again with the target, and this introduces artificial noise into the contact forces. To reduce these noises, a "regularization" strategy has been implemented by Stoll and Brockman [22] to gradually impose the contact constraint as a node descends through a buffer zone above the contact surface, and solid tetrahedral elements to model the bird. As a result, a refined mesh is highly desirable to reduce this type of artificial oscillations, although this inevitably increases the CPU time. To circumvent element deletion, Langrand et al. [27] attempted another technique, namely, the mass scaling of the bird elements by increasing the local mass density ρ deliberately to keep the time step constant. However, this inadvertently causes the mass of the bird to become several hundred times greater than the original bird at the final time step.

In view of the recent rapid advancement in high-performance computing (HPC), the strategy of employing dense meshes can be

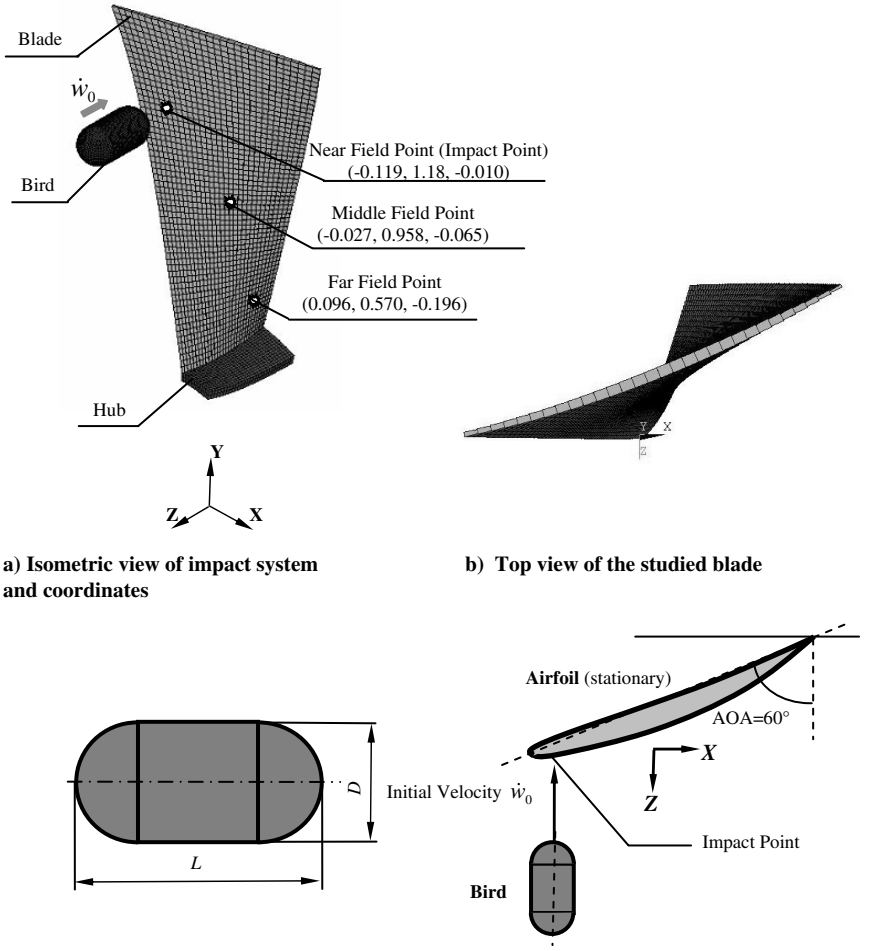

a) Isometric view of impact system and coordinates

b) Top view of the studied blade

c) Hemispherical-ended cylinder configuration used to model bird

d) Schematic diagram of impacting scenario

Fig. 1 Finite element model of an artificial bird striking a fan blade.

used to alleviate the problems associated with Lagrangian formulations. Modern HPC systems can tolerate very small time steps of 10^{-9} s or even 10^{-10} s, whereas it used to be 10^{-6}–10^{-7} s just a few years ago. Thus, by refining the mesh of the Lagrangian bird, the artificial oscillations associated with the impact force are expected to be reduced to negligible levels.

In addition to the canonical Lagrangian formulation, there are other methods such as the Eulerian and arbitrary Lagrangian Eulerian (ALE) approaches. A very refined mesh is usually required for the Eulerian method to capture the material response, making it very computationally expensive. The ALE approach, on the other hand, suffers significant numerical dissipation and the solid–fluid interface is also rather difficult to describe in cases involving rotating blades. As reported by Anghileri et al. [28], the meshes used in discretizing the bird were extremely distorted so that the accuracy of the ALE approach become questionable, even when they were refined at the

Table 1 Properties used in validation test

Bird	Target
$m = 1.82$ kg, $\rho_0 = 934.3$ kg/m^3, $\dot{w}_0 = 225$ m/s	Rigid plate

Table 2 Bird strike reference case

Bird	Target
$m = 1.82$ kg, $\rho_0 = 943$ kg/m^3, $\dot{w}_0 = 225$ m/s	Flexible engine fan blade $E = 1.14 \times 10^{11}$ Pa, $\nu = 0.33$, $\rho_{\text{blade}} = 4.429 \times 10^3$ kg/m^3 $\sigma_y(\varepsilon^P_{\text{eff}}) = 1.14 \times 10^8$ Pa

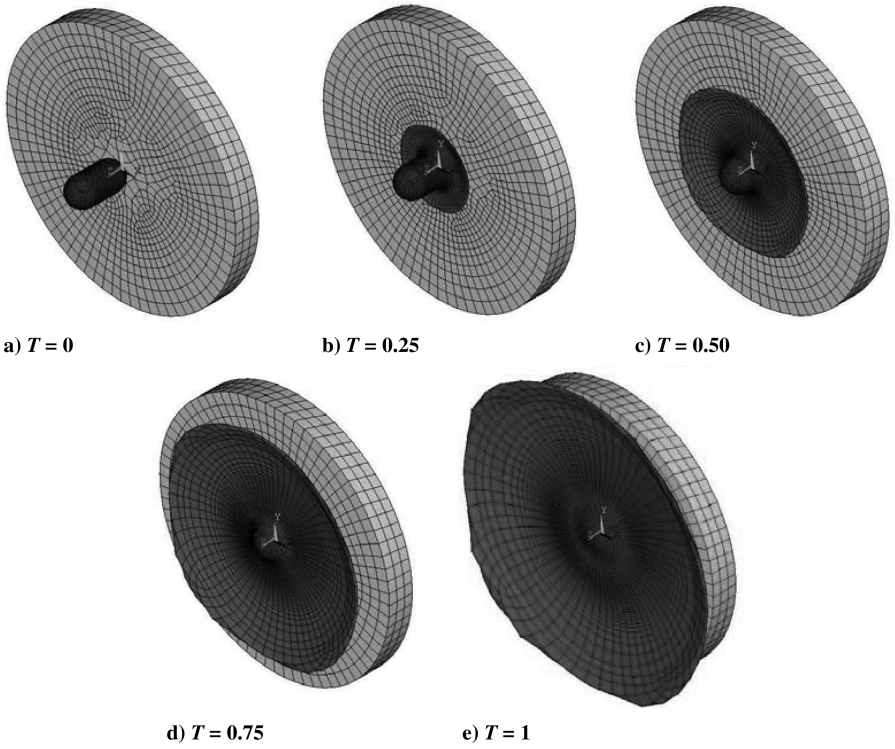

a) $T = 0$ **b) $T = 0.25$** **c) $T = 0.50$**

d) $T = 0.75$ **e) $T = 1$**

Fig. 2 Deformation history of a bird striking a rigid target.

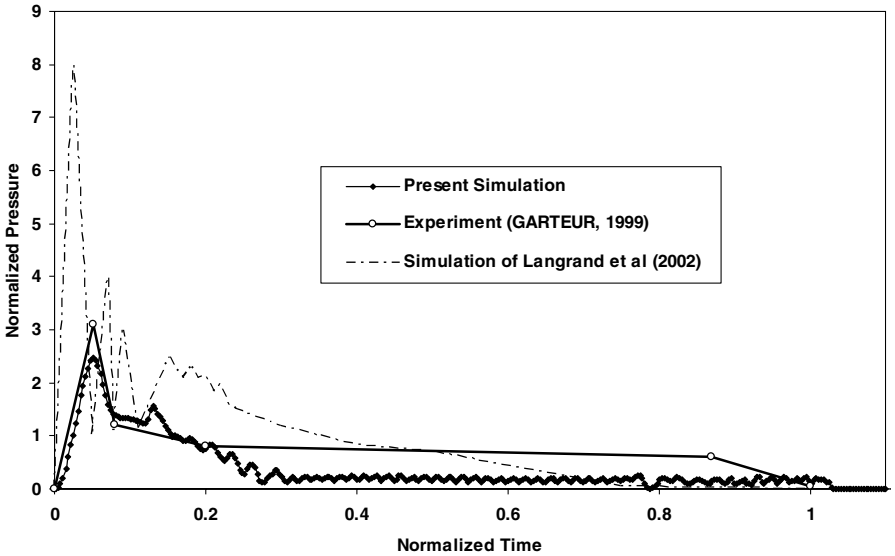

Fig. 3 Variation of normalized pressure vs normalized time.

contact interface. Other researchers, such as Langrand et al. [27], also compared the Lagrangian with the ALE approach for bird strike simulations and reached the same conclusion: specifically, the ALE is less accurate.

Besides the finite element method, the discrete element methods (DEMs) have also been developed and implemented for large deformation simulations, such as Feng et al. [29]. Sometimes the coupled finite/discrete elements provide more accurate results: for example, in the analysis of shot peening processes [30]. Two notable DEMs, namely, the nodal masses (NM) model and smooth particle hydrodynamics (SPH), have been found suitable for bird strike simulations. However, the NM method neglects the bird deformation contribution on the energy absorbing mechanism [23]. The meshless SPH method, which is relatively new, was first developed for hypervelocity impact simulations such as orbital debris impacting problems [31] that result in large deformations and displacements, by introducing variable nodal connectivity. However, its drawback is that the connectivity between particles has to be calculated repeatedly [19].

Customarily, the geometry of the bird torso can be simplified to be a hemispherical-ended cylinder [17]. The mechanical properties of the bird tissue actually change from low-velocity to high-velocity ranges. Strictly speaking, the mechanical property of avian tissue at low speeds is anisotropic and inhomogeneous. Fortunately, this anisotropy and inhomogeneity becomes progressively negligible as the speed increases, and at sufficiently high speeds, the bird can actually be considered as a compressible jet of fluid impinging on the structure [3]. Thus, canonical constitutive law of homogenized fluidic materials can therefore be used, such that

$$\sigma_{ij} = -P\delta_{ij} + 2\rho\gamma\dot{e}_{ij} \tag{2}$$

Different hydrodynamic models have been successfully used to describe the material properties of the bird in compression (for $\mu < 0$), among which the most commonly used is the polynomial form of state,

$$P = C_0 + C_1\mu + C_2\mu^2 + C_3\mu^3 \tag{3}$$

in which μ is the mass density changing ratio

$$\mu = \frac{\rho}{\rho_0} - 1 \tag{4}$$

with ρ and ρ_0 being the instantaneous and initial mass densities of the bird, respectively. Through this hydrodynamic modeling, one is able to avoid the disintegration of the bird model into numerous particles.

In earlier works, bird strike simulations have been carried out on different forward-facing components of the aircraft, such as the aircraft transparency and canopy [32–34], the leading edges of wings or empennages [26,35], the wing slats [36], the radome [37], the

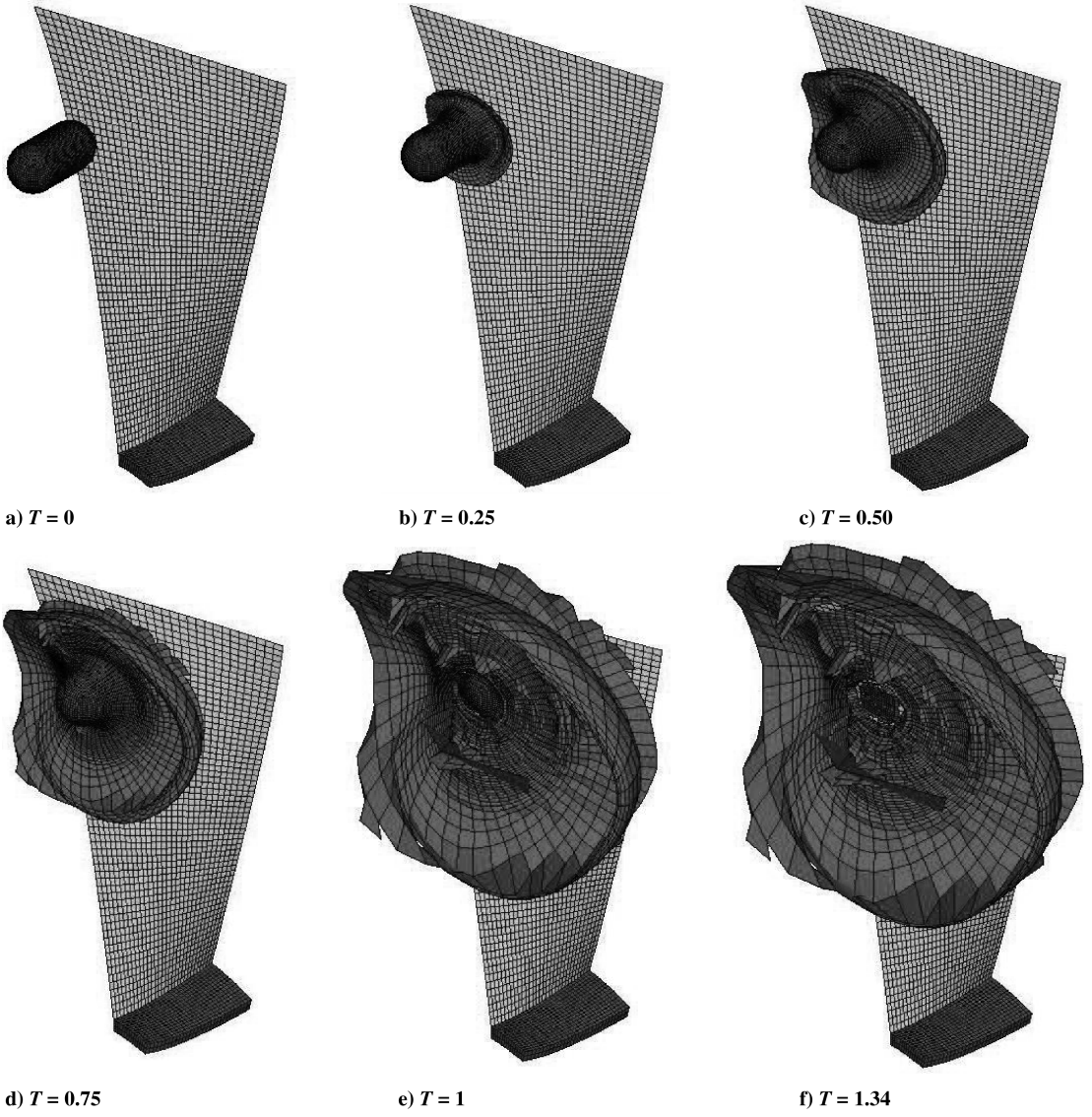

Fig. 4 Deformation history of a bird striking a flexible fan blade.

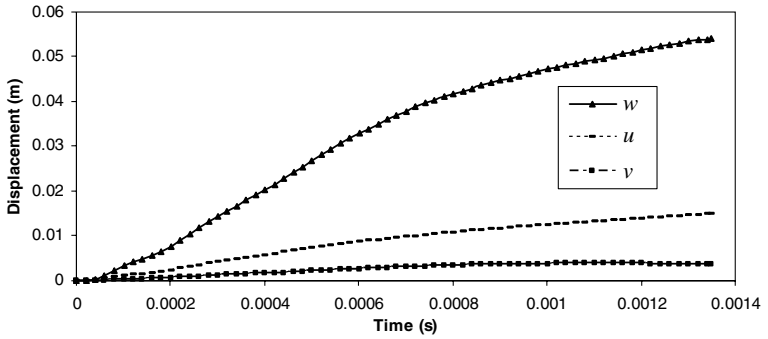

a) Displacements in X, Y, Z directions

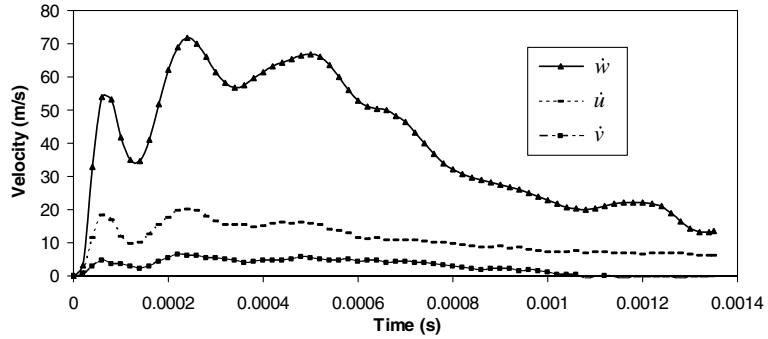

b) Velocities in X,Y, Z directions

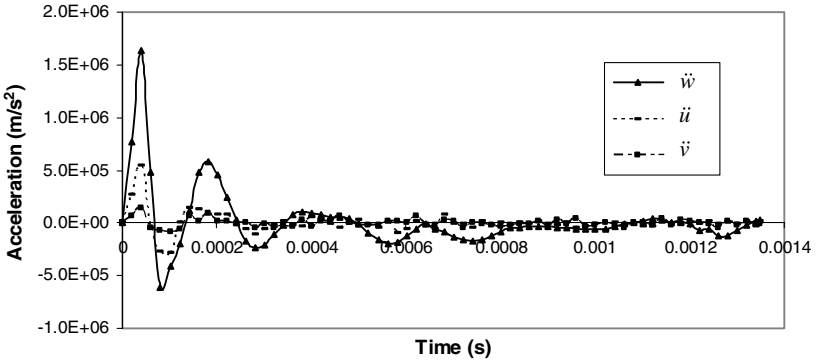

c) Accelerations in X, Y, Z directions

Fig. 5 Time histories of displacement, velocity, and acceleration of near-field point.

fuselage [38], and the intake of a turbofan engine [28]. A strong consensus which has been reached is that the constitutive characteristics of both the bird and the aircraft components play key roles in determining the impacting forces and the extent of the resulting damage.

In this paper, we employ explicit 3-D finite element analysis (LS-DYNA) to carry out comprehensive studies on the transient nonlinear responses of bird strike on a flexible fan blade. The effects of different impact velocities are simulated and important elements such as the impact forces and the energies of the bird–blade interaction are examined and discussed. Because of the scarcity of data on large bird strike, strikes involving larger birds are also investigated in details here. The size effect can be significant, as indicated by Reddy [39] in the case involving metal–metal hypervelocity impact analyses.

II. Finite Element Modeling

A. Discretized Blade Model

In the present simulation, we use one sector of the fan composed of a single blade and a hub section, as shown in Fig. 1a, together with the bird model. The hub was assumed rigid in comparison with the blade. In the present investigation, Shell-163 element in LS-DYNA was used to simulate the blade with 31 nodes in the axial direction and 61 nodes in the radial direction.

In addition, the Hughes–Liu formulations were used to eliminate certain hourglass modes. The thickness of the selected blade (shown in Fig. 1b) varies according to the following relation:

$$\Delta = 0.026 - 0.00463y^2 - (z + 0.1)^2 \tag{5}$$

which is typical of fan blade dimensions in commercial wide-bodied aircrafts.

Fan blades are typically made of Titanium alloy Ti-6Al-4V. Because of the high strain rates associated with this problem, the selected constitutive law was of the viscoplastic type devised originally by Perzyna [40], and used by Cowper-Symonds in impact problems, viz.,

$$\sigma_y(\varepsilon^P_{\text{eff}}, \dot{\varepsilon}^P_{\text{eff}}) = \sigma_y(\varepsilon^P_{\text{eff}}) \left[1 + \left(\frac{\dot{\varepsilon}^P_{\text{eff}}}{C}\right)^{\frac{1}{P}}\right] \tag{6}$$

where $\dot{\varepsilon}^P_{\text{eff}}$ is the effective plastic strain rate, C and P are strain rate parameters which are experimentally determined, and $\sigma_y(\varepsilon^P_{\text{eff}})$ is the initial quasi-static yield stress. These data are listed in Table 2.

B. Discretized Bird Model

In our investigations, the bird was modeled as a cylinder with hemispherical ends, as shown in Fig. 1c. Furthermore, the Brockman model [33] with waterlike constitutive law, depicted in Eq. (3), was

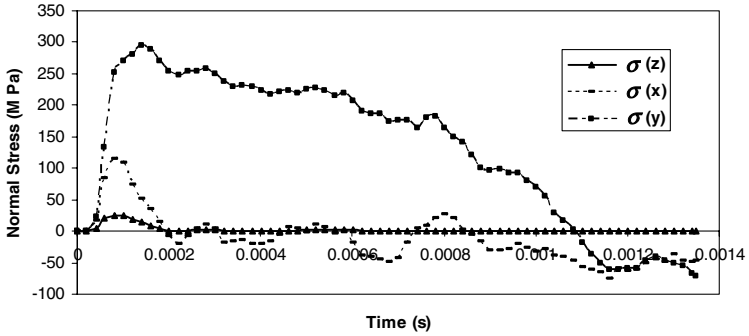

a) Normal stresses in X, Y, Z directions

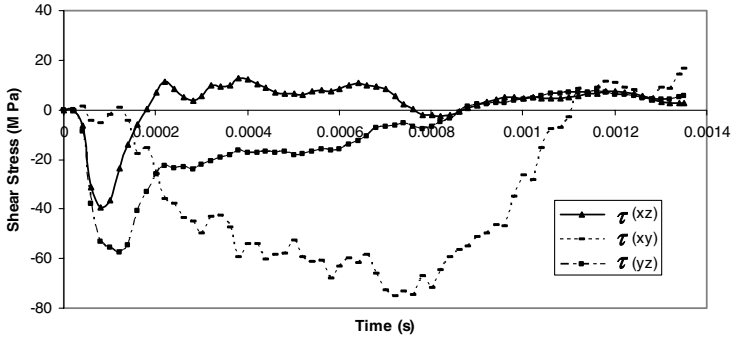

b) Shear stresses in XY, YZ, XZ planes

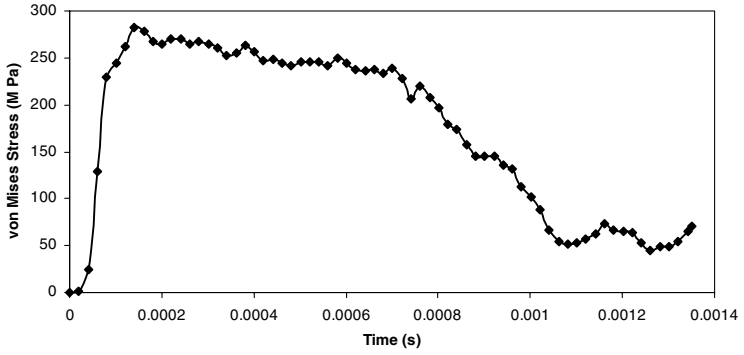

c) von Mises stress

Fig. 6 Normal, shear, and von Mises stresses of near-field point.

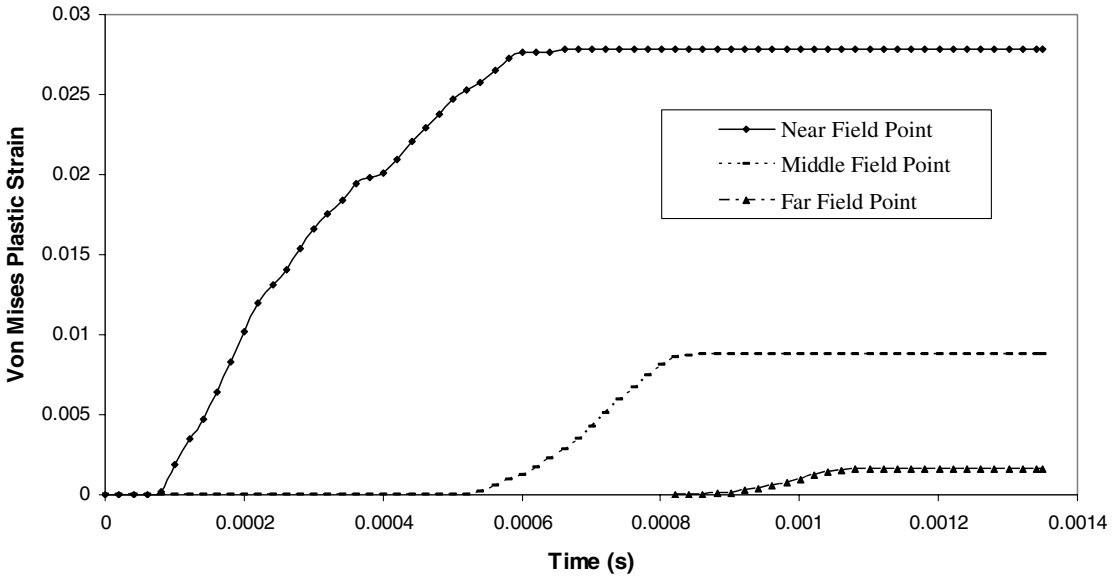

Fig. 7 von Mises plastic strain histories of near-, middle-, and far-field points.

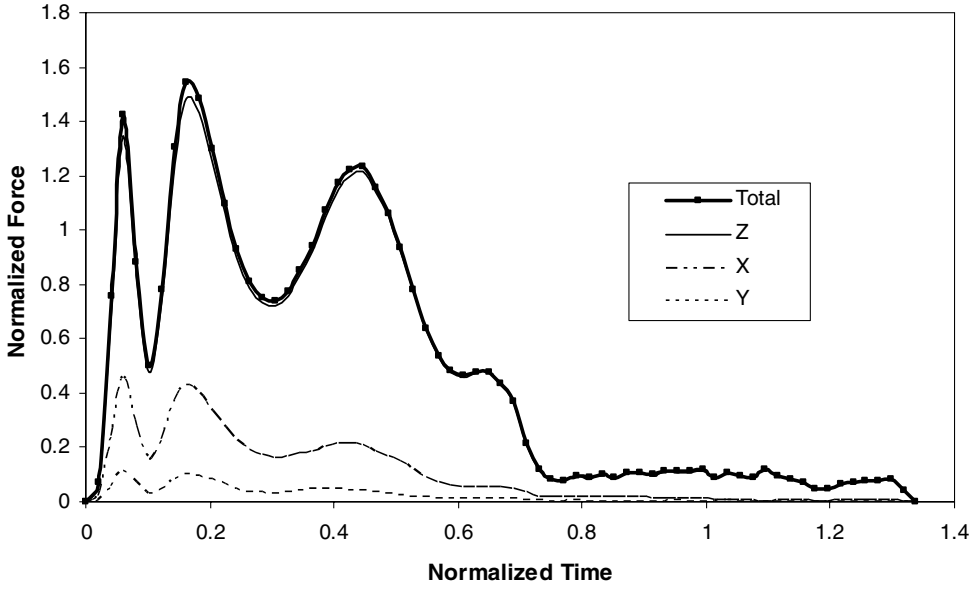

a) Normalized impact forces

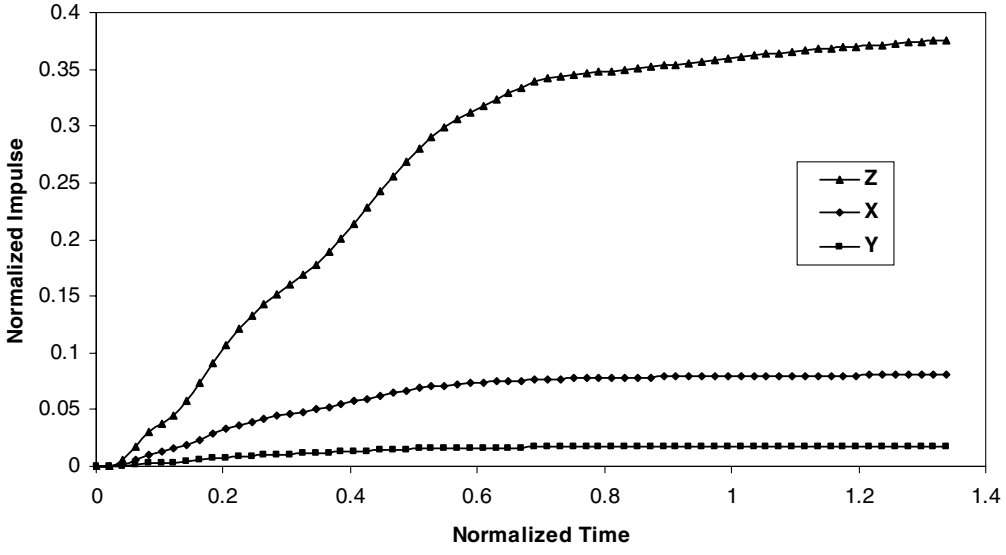

b) Normalized impulse

Fig. 8 Impact forces and impulse variations for the considered reference case.

adopted. The compressible modules selected herein were those due to Brockman and Held [33]:

$$C_0 = 0, \qquad C_1 = 2323 \text{ MPa}, \qquad C_2 = 5026 \text{ MPa}, \qquad C_3 = 15180 \text{ MPa} \tag{7}$$

Eight-node solid elements (ANSYS Solid-164) were used for the bird model. In these simulations, the hourglass energy should be limited within a certain range (usually under 10%) to achieve good results. The Solid-164 elements were found to provide good hourglass control. The impact scenario is schematically shown in Fig. 1d. The automatic surface-to-surface contact is defined between the bird and target. For ease of subsequent comparison between the present numerical results and those (experimental and numerical) reported by other independent researchers, various normalized parameters have been introduced, and these have been defined in the nomenclature.

III. Results and Discussions

A. Validation of Results

The aim of this test is to assess the accuracy and validity of the finite element blade and bird models. It involves a single 4 lb (1.82 kg) bird, the properties of which are listed in Table 1. In this case, we selected a bird velocity of 225 m/s striking a stationary large rigid target at normal incidence. As indicated earlier, the bird is modeled as a cylinder with hemispherical ends, with length-to-diameter ratio of 2. Convergence tests pertaining to mesh density and integration time steps were carried out, and it was found that 39,424 hexahedral elements were required to model the bird. In the convergence test carried out, when the number of elements for the bird model was refined from 26,412 to 39,424, the result in terms of global impact force changed by less than 4%.

The normalized time histories 0, 0.25, 0.50, 0.75, and 1 of the benchmark bird striking a rigid target are depicted in Fig. 2. The hydrodynamic fluidlike behavior of the bird can be clearly observed in that figure, especially at the higher normalized times. Figure 3

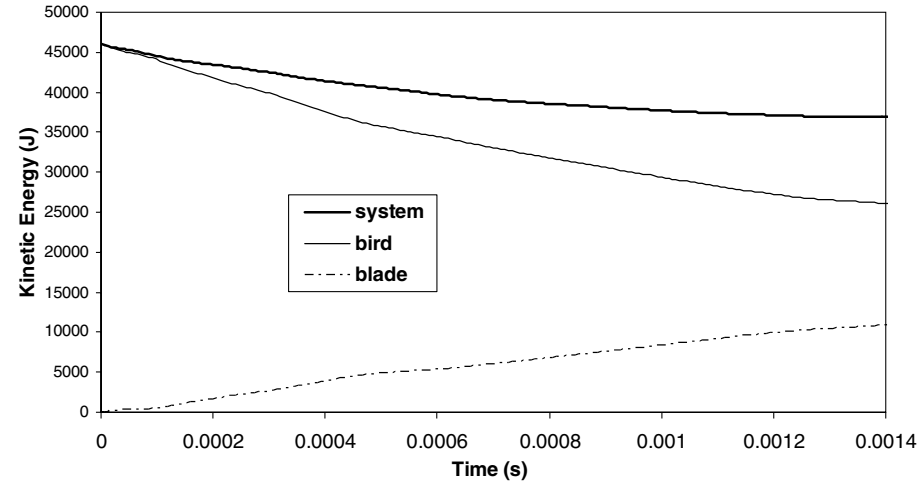

a) Kinetic energy

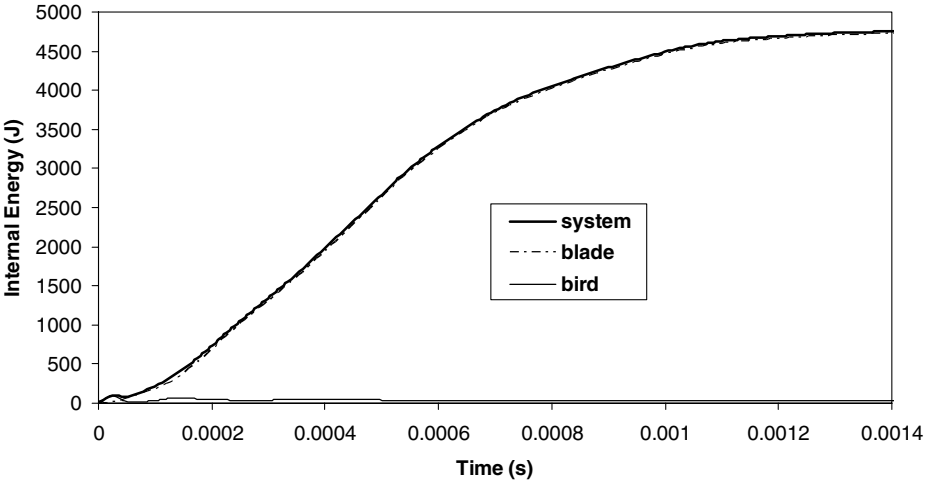

b) Internal energy

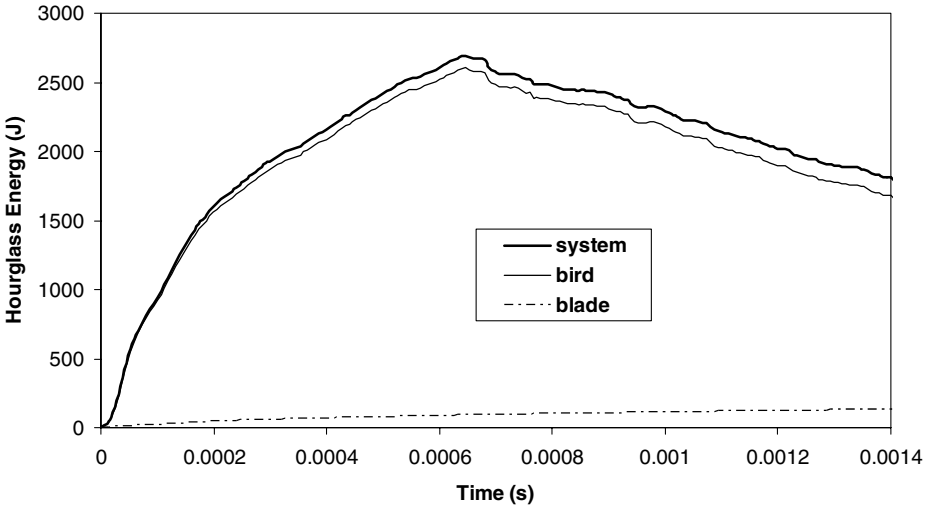

c) Hourglass energy

Fig. 9 Kinetic, internal, and hourglass energies for the reference case.

shows the variation of the normalized pressure against time. It is compared with the experimental data from the GARTEUR Bird Strike Group [41] and the numerical results of Langrand et al. [27]. It is clearly observed from the figure that the present numerical results correspond quite well with the experimental data. If compared with the simulation results reported in the literature, our work indicates fewer oscillations than those prevalent in earlier studies, and appears to be more stable. This is attributed to the fine mesh density used in discretizing the geometries used in the present investigation. Specifically, we used bird-to-element length ratio of about 30, as compared to 8 used in literatures [22,26]. The peak value of the pressure from the present simulation is about 20% lower than that of

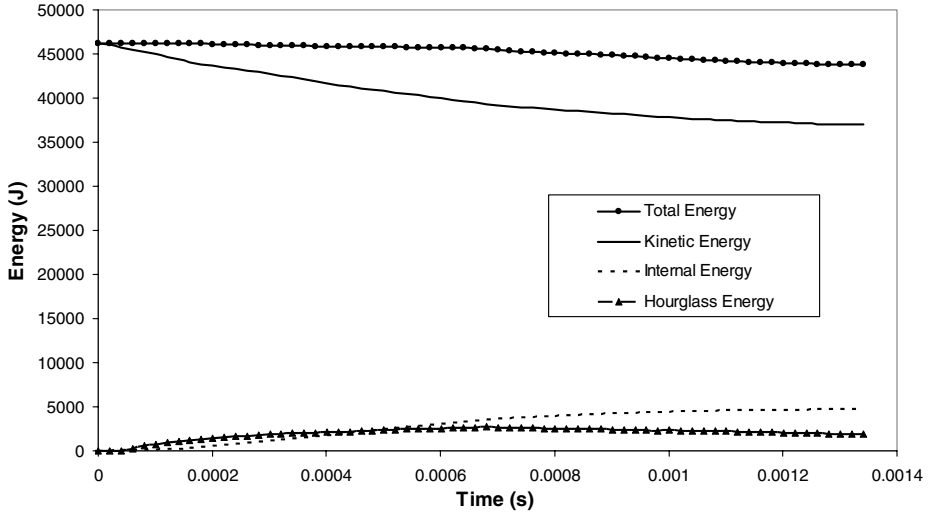

Fig. 10 Energy distributions of the bird–blade system for the reference case.

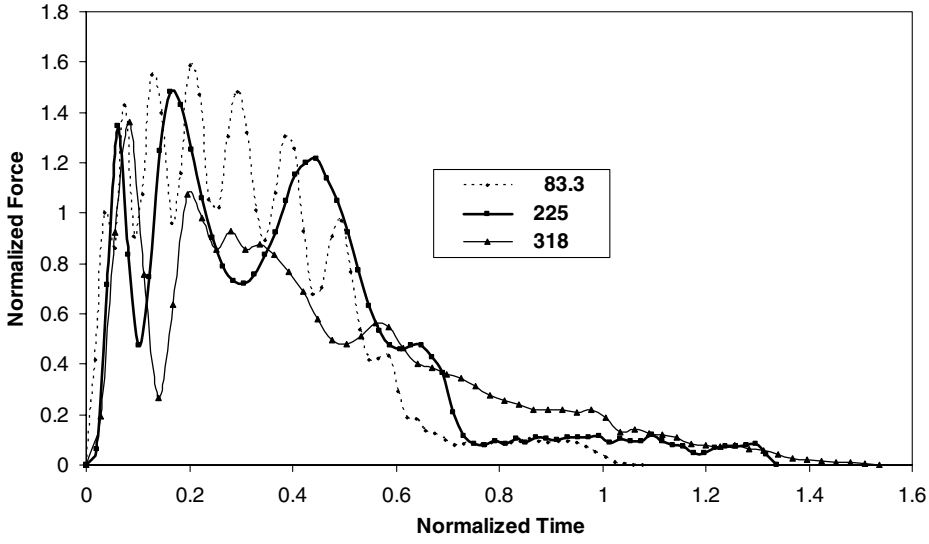

Fig. 11 Normalized impact forces for different impact velocities.

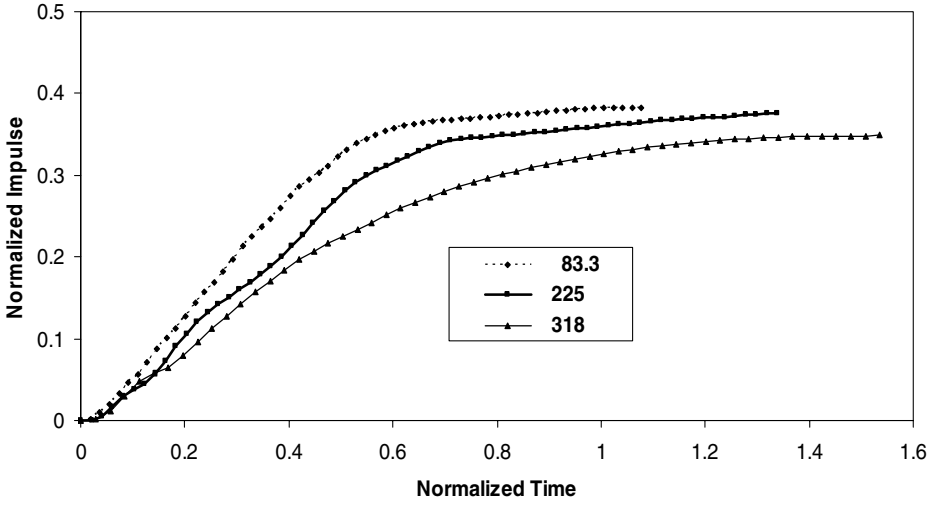

Fig. 12 Normalized impulse values for different impact velocities.

the experimental data, and this difference is probably due to the use of water compressible modules for the bird's material model. It is expected that these values underestimate the behavior of a real bird.

B. Parametric Studies

The reference case for a bird striking a flexible fan blade is studied with a 4 lb (1.82 kg) bird having an initial impact velocity of 225 m/s

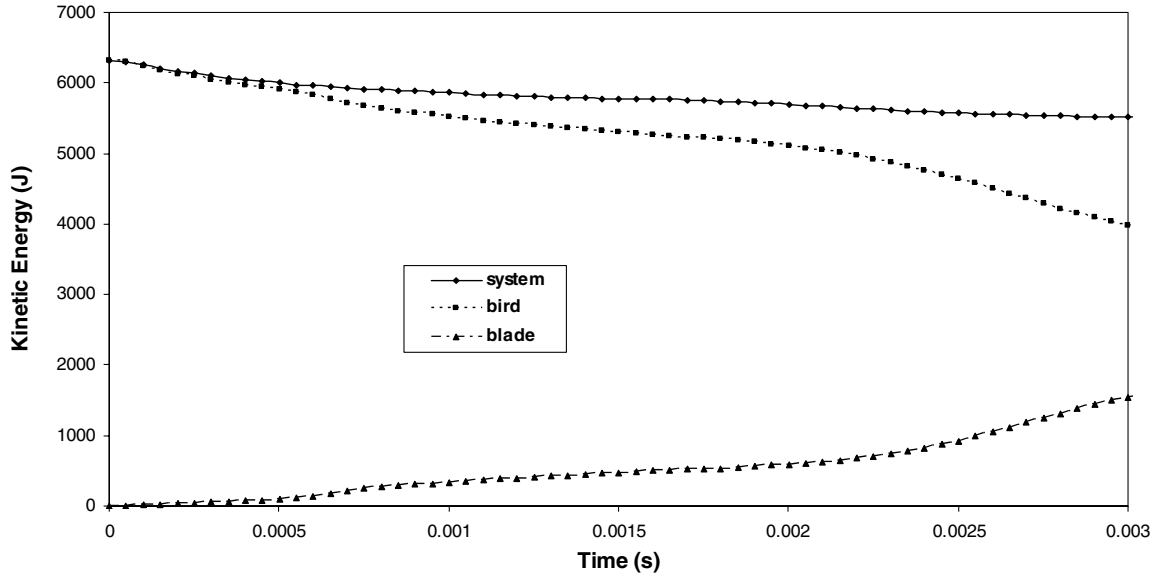

a) Kinetic energy

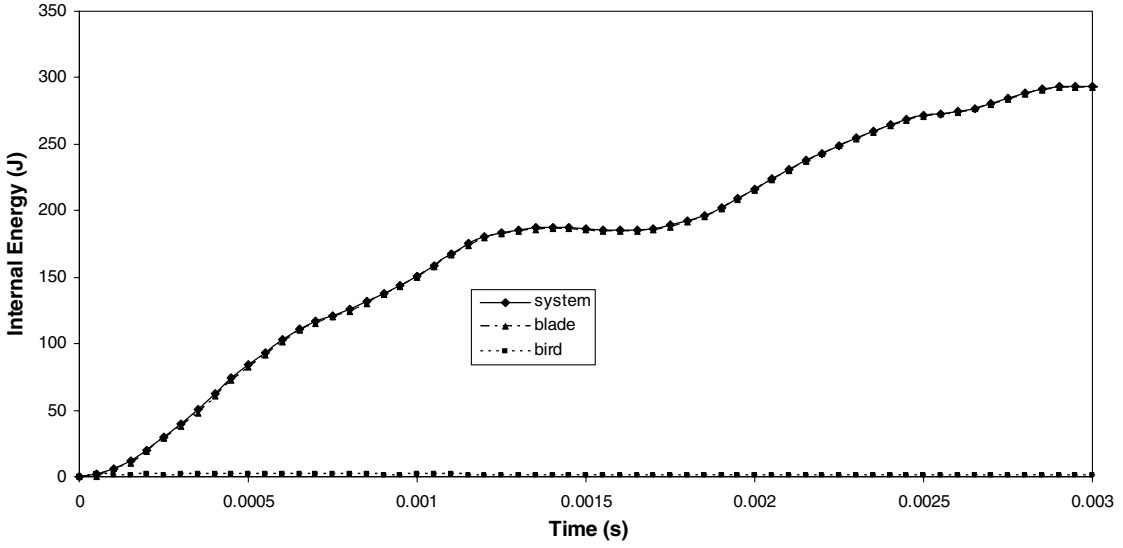

b) Internal energy

Fig. 13 Kinetic and internal energies for an initial impact velocity of 83.3 m/s.

and the properties listed in Table 2. The point of impact, as shown schematically in Figs. 1a and 1d, is located at 85% of the radius away from the center of rotation, and the angle of attack (AOA) of the inclined airfoil at this location as shown in Fig. 1d is 60 deg. Three points on the blade, corresponding to their relative vicinity to the point of impact, have been designated for more detailed examination. These points are the near-field, middle-field, and far-field impact points, and their coordinates are provided in Fig. 1a.

Sample time histories of the deformation of the blade and bird for this selected reference case are shown in Fig. 4. The figure clearly shows the evolution of the bird deformation during impact. The severity of the localized contact at the initial stages of impact will lead to plastic deformation in the considered blade. The displacements, velocities, and accelerations in x-, y-, and z-directions of one blade point in the near field of the impact region are shown in Fig. 5. As expected, the displacements, velocities, and accelerations in x- and y-directions are much lower than those in the z-direction. The maximum velocity of this near-field point in the z-direction is as high as 32% of the initial bird velocity. The maximum instantaneous acceleration is found to be 1.6×10^6 m/s^2 occurring just after impact and decreases quite rapidly.

Figure 6 shows the time histories of the normal, shear, and von Mises stresses. Because of the bending of the blade, the normal stresses in the y-direction are of the highest magnitude, whereas those in the x- and z-directions are considerably lower. The maximum normal stress in the y-direction is found to be about 295 MPa. The shear stresses are almost one order lower than the normal stresses at that point. Consequently, the von Mises stresses reflect the influence of the dominant σ_Y stress.

Figure 7 plots the von Mises plastic strains of three representative points. The von Mises plastic strain of the near-field point is several times larger than that of the middle-field point, which is in turn larger than that of the far-field point. The maximum von Mises plastic strain is about 0.028, which is found to be approximately 10 times of its corresponding elastic strain.

The impact force and impulse variations in the x-, y-, and z-directions are shown in Fig. 8. As in the case of the respective velocities and accelerations, the impact forces in the x- and y-directions are much lower than the impact force in the z-direction, which is almost of the same magnitude as the total impacting force. As such, in the subsequent results presented, only the impact force in the z-direction is considered. The maximum normalized impact force in that direction is found to be 1.48, which is equivalent to about 360 kN. From the impulse plot, we also observe that the momentum is transmitted from the bird to the blade gradually throughout the impact duration. Because of the fixed boundary conditions of the

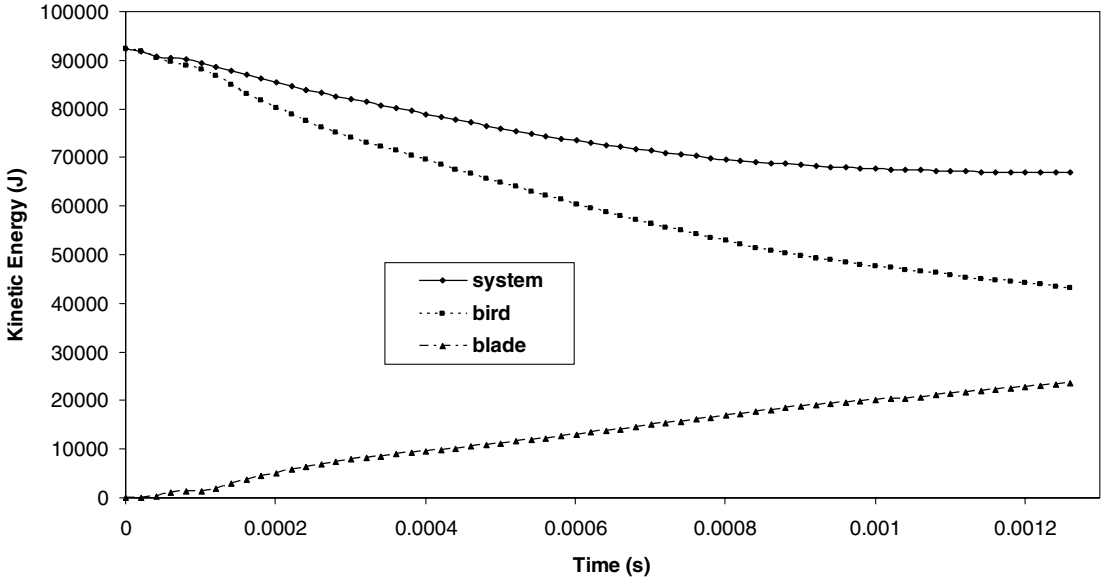

a) Kinetic energy

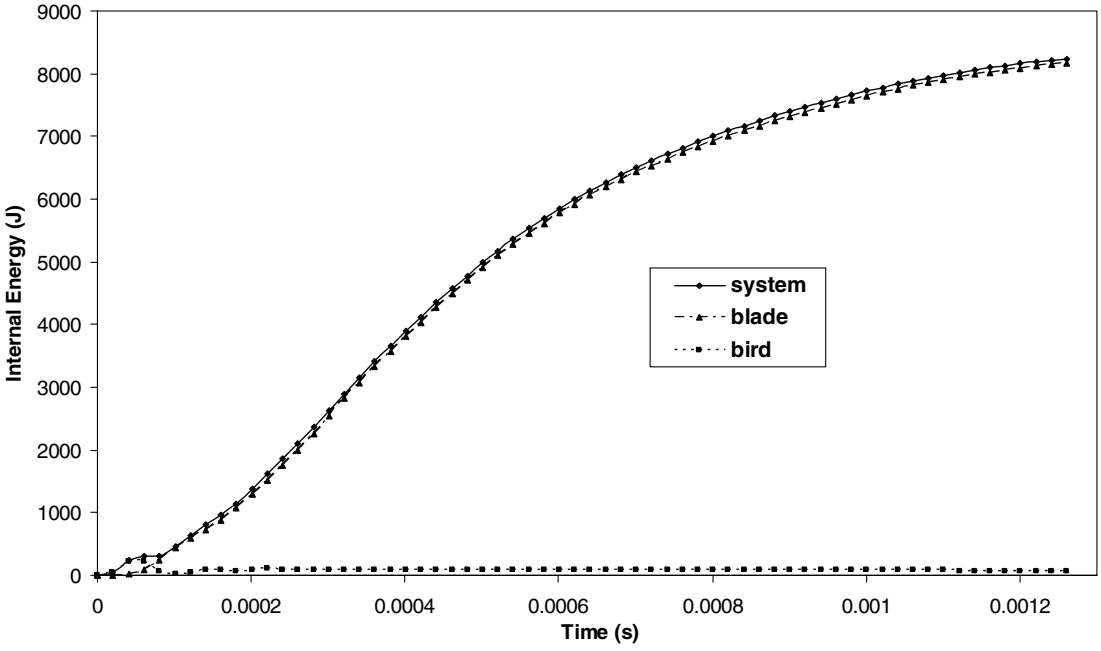

b) Internal energy

Fig. 14 Kinetic and internal energies for an initial impact velocity of 318 m/s.

blade, losses result and only 37.5, 8.0, and 1.7% of the initial momentum of the bird are transmitted to the blade in the z-, x-, and y-directions, respectively. The present simulation is most successful in suppressing the stairway profiles during the process of the impulse accumulation, which was observed in the simulation of Stoll and Brockman [22] due to the presence of undesired spiky contact force histories in their results.

The kinetic, internal, and hourglass energies of the bird, blade, and the system that is composed of both the bird and blade, have been plotted in Fig. 9. The kinetic energy is transmitted from the bird to the flexible blade gradually. Meanwhile, the total kinetic energy decreases, as it is transformed into internal energy in the flexible blade, as can be seen from Fig. 10. The internal energy of the blade is found to be much larger than that of the bird, and this is due to the inelastic fluidlike properties of the bird elements. On the other hand, the hourglass energy of the bird is significantly higher than that of the blade. This is because the bird has been modeled using eight-node brick elements, whereas the blade is modeled using Hughes–Liu formulated shell elements, which possess hourglass control. In the present analysis, the hourglass energy of the whole system is only 6% (or less) of the total energy.

C. Effects of Bird Impact Velocity

The initial impact velocity of the bird was varied from 83.3 m/s to 318 m/s, with the geometrical and physical properties of the bird being the same as those of the parametric tests. The velocities considered for the bird cover the normal velocity range of commercial airplanes in flight. The normalized impact forces are shown in Fig. 11 for the respective velocities 83.3, 225, and 318 m/s. The maximum normalized forces for these three cases are 1.59, 1.48, and 1.36, respectively. For the case of $\dot{w}_0 = 83.3$ m/s, the impact force drops to relatively low magnitudes at about normalized time $T = 0.7$, and vanishes at $T = 1.08$. It is also noted that there are more oscillations in the impact force compared to the other two higher velocity cases considered. As for the case of $\dot{w}_0 = 318$ m/s, the force reaches its maximum value and then gradually decreases while slightly oscillating until it vanishes at

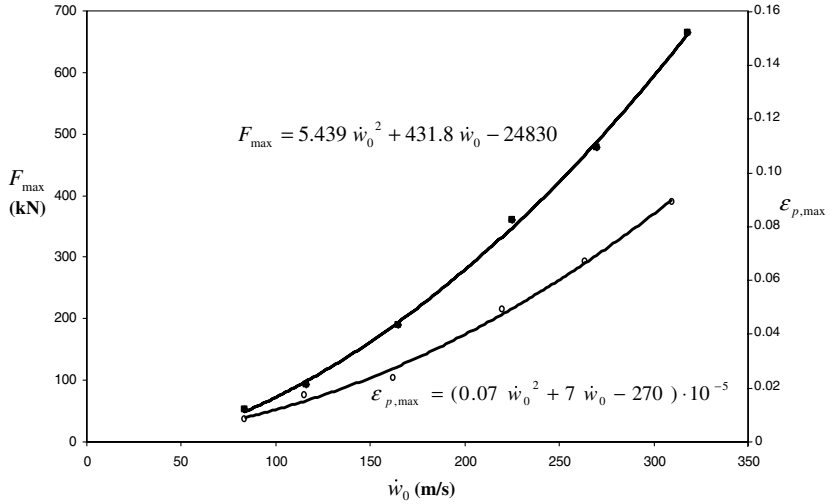

Fig. 15 Variations of maximum impact force and plastic strain with initial impact velocity.

$T = 1.54$. The impulses resulting from these three velocity cases are plotted in Fig. 12. The impulse variations for the three cases considered exhibit the same trend. Because the mass of the bird remains constant, normalization of the impulse equations effectively meant the division by $\dot{w}_0$. Accordingly, when the impulse values are normalized by their corresponding initial impact velocity $\dot{w}_0$, the higher velocities result in overall lower normalized impulse curve.

The kinetic and internal energies for the bird, blade, and the bird–blade system are shown in Figs. 13 and 14 for the cases of $\dot{w}_0 = 83.3$ m/s and $\dot{w}_0 = 318$ m/s, respectively. Together with Fig. 9 for the case of $\dot{w}_0 = 225$ m/s, the energy transfer rate between the bird and blade can be observed to be higher at higher impact velocities. Furthermore, it can be deduced from Fig. 15 that the maximum impact force between the bird and the blade increases in a parabolic manner with velocity. Their relationship can be approximated as

$$F_{max} = 5.439\dot{w}_0^2 + 431.8\dot{w}_0 - 24830, \quad (318 \geq \dot{w}_0 \geq 83.3\ \text{m/s}) \tag{8}$$

It should be noted that this relationship is not general but specific to the presently described bird strike case. In addition, with the increase of the impact velocity, the maximum plastic strain of the blade increases as well due to higher striking forces from the bird, and follows the following relationship for the presently considered case:

$$\varepsilon_{p,max} = (0.07\dot{w}_0^2 + 7\dot{w}_0 - 270) \times 10^{-5}, \quad (318 \geq \dot{w}_0 \geq 83.3\ \text{m/s}) \tag{9}$$

which is also shown in Fig. 15.

D. Effects of Bird Size

The normal ingestion standard of using 4 lb (1.82 kg) birds for aeroengine strikes inevitably leaves out many large flocking bird species. To investigate the effects of heavier bird strikes, 6 lb (2.72 kg) and 8 lb (3.63 kg) birds are considered here. The mass density of bird models, with feathers removed, has been enumerated by the databases of the International Birdstrike Research Group [42] as

$$\rho_0 = 1148 - 63 \times \log_{10}(1000 \times m) = 959 - 63 \times \log_{10}(m) \tag{10}$$

where m and ρ_0 are, respectively, the mass and initial density of the bird in SI units. The diameter of the bird model is

$$D = 2\left(\frac{m}{2\pi\rho_0}\right)^{\frac{1}{3}}\left(\frac{L}{D} - \frac{1}{3}\right)^{-\frac{1}{3}} \tag{11}$$

where L/D is the length-to-diameter aspect ratio. Based on the relationships of Eqs. (10) and (11), the lengths and diameters of 6 lb (2.72 kg) and 8 lb (3.63 kg) birds can be obtained and these data are listed in Table 3.

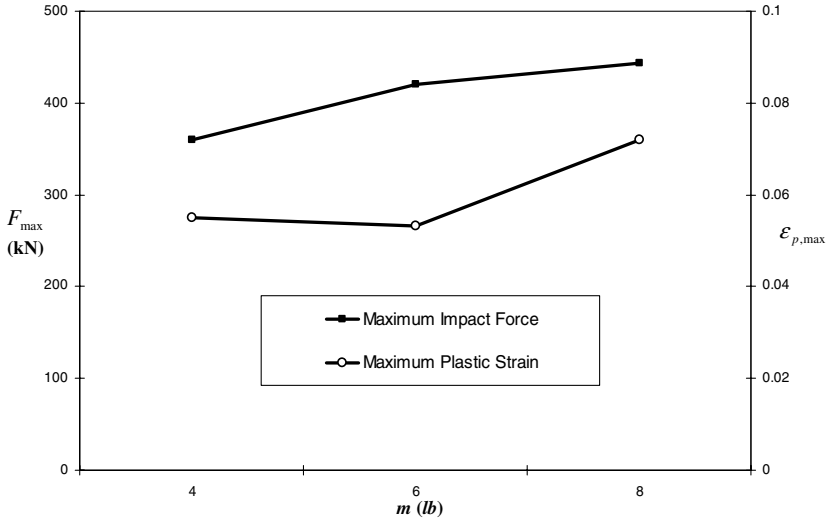

Fig. 16 Maximum impact force and plastic strain for birds with different masses.

Table 3 Large bird properties

Mass m, lb (kg)	Initial mass density ρ_0, kg/m^3	Length L, m	Diameter D, m
4 (1.82) (parametric test)	943	0.228	0.114
6 (2.72)	932	0.262	0.131
8 (3.63)	923	0.288	0.144

In this investigation, hemispherical-ended cylinder models with aspect ratio 2 are employed to simulate the heavier birds. In this case, the initial velocity of the birds is taken to be 225 m/s and impinging at an angle of attack of 60 deg. As expected, Fig. 16, the maximum impact force increases with the mass of the bird. However, it is also noted that the increase rate decreases slightly due to the lower density effect dictated by Eq. (10). In addition, the maximum plastic strain of the blade struck by a 6 lb (2.72 kg) bird is found to be even less than that experienced by the 4 lb (1.82 kg) bird. This again can be attributed to the reduced density of the heavier bird, which decreases logarithmically with respect to the mass of the bird. Thus, it is clearly observed here for the case of larger bird strikes that the heavier masses and corresponding lower densities play opposite roles in the resultant global impact forces and plastic strains.

IV. Conclusions

With the advent of large fan engines with increased frontal areas and no inlet guide vanes, the understanding of the bird strike problem and its proper mitigation now take on even more significance. Whereas manufacturers undertake a great deal of in-house testing before certification, it is also highly desirable to have predictive numerical models to assess the bird impact resistance of new generation engine fan blades. To validate the present finite element formulation, comparison with reported experimental data for a bird striking a rigid target was carried out. It was found that the hydrodynamic Lagrangian bird is appropriate for the bird strike simulation considered in this study. Subsequently, a bird strike reference case was developed to carry out parametric studies, and this was followed by studies to examine the effects of different impact velocity magnitudes on the fan blade. The results reveal that increasing initial impact velocity leads to an increase in the maximum impact force and the maximum plastic strain. Finally, larger birds heavier than the present standard 4 lb (1.82 kg) were examined. It was found that the maximum impact force increased with larger/heavier birds, but this trend is not necessarily so for the maximum plastic strain of the blade due to the reduced density of the impacting bird.

Acknowledgment

The authors wish to acknowledge the kind support of DSO laboratories, Singapore.

References

[1] French, R. F., "Test Techniques and Equipment for the Development of Air Craft Engine Components Resistant to Bird Ingestion," ASME Paper, Vol. 19, 1974, pp. 20–26.

[2] Barber, J. P., Taylor, H. R., and Wilbeck, J. S., "Bird Impact Forces and Pressures on Rigid and Compliant Targets," University of Dayton Research Institute, Technical Report AFFDL-TR-77-60, Dayton, OH, 1978.

[3] Wilbeck, J. S., "Impact Behavior of Low Strength Projectiles," Air Force Materials Lab, Air Force Wright Aeronautical Labs, Report No. AFML-TR-77-134, Wright–Patterson AFB, OH, 1977.

[4] Reddy, J. N., "Finite Element Analysis of the Initial Stages of Hypervelocity Impact," *Computer Methods in Applied Mechanics and Engineering*, Vol. 9, No. 1, Sept. 1976, pp. 47–63.

[5] Wilbeck, J. S., and Rand, J. L., "The Development of a Substitute Bird Model," ASME Paper 81-GT-23, 1981.

[6] Richard, B., "The Development of a Substitute Artificial Bird by the International Bird Strike Research Group for Use in Aircraft Component Testing," International Bird Strike Committee Paper ISBC25/WP-IE3, Amsterdam, 2000.

[7] Aiello, R. A., Hirschbein, M. S., and Chamis, C. C., "Structural Dynamics of Shroudless, Hollow Fan Blades with Composite In-Lays," ASME Paper 82-GT-284, 1982.

[8] Shioya, T., and Stronge, W. J., "Impact Bending of a Rotating, Rigid-Plastic Fan Blade," *Journal of Propulsion and Power*, Vol. 1, No. 5, 1985, pp. 375–380.

[9] Schuette, W., "Blade Behavior During Bird Strike," *Science and Engineering on Supercomputers, Proceedings of the 5th International Conference*, 1990, pp. 145–157.

[10] Miyachi, T., Okumura, H., and Ohtake, K., "Analysis of the Effect of Centrifugal Force on the Impact Resistance of Composite Fan Blades for Turbo-Fan Engines," *Proceedings of Society of Automotive Engineers*, No. P-246, 1991, pp. 619–626.

[11] Alexander, A., "Interactive Multi-Mode Blade Impact Analysis," ASME Paper 81-GT-79, 1981.

[12] Yu, J. L., and Jones, N., "Numerical Simulation of Impact Loaded Steel Beams and the Failure Criteria," *International Journal of Solids and Structures*, Vol. 34, No. 30, 1997, pp. 3977–4004.

[13] Martin, N. F., "Nonlinear Finite-Element Analysis to Predict Fan-Blade Damage due to Soft-Body Impact," *Journal of Propulsion and Power*, Vol. 6, No. 4, 1990, pp. 445–450.

[14] Gao, D. P., and Li, Q. H., "Analytical and Experimental Investigation of Bird Impact on Blades," *Journal of Aerospace Power*, Vol. 5, No. 4, 1990, pp. 335–338.

[15] Teichman, H. C., and Tadros, R. N., "Analytical and Experimental Simulation on Fan Blade Behavior and Damage Under Bird Impact," *Journal of Engineering for Gas Turbines and Power*, Vol. 113, Oct. 1991, pp. 582–594.

[16] Lawson, M., and Turley, R., "Supercomputer Simulation of a Birdstrike on a Turbofan Aero Engine," *Finite Element News*, No. 3, June 1987, pp. 10–14.

[17] Frischbier, J., "Bird Strike Capability of a Transonic Fan Blisk," *Proceedings of the ASME Turboexpo 1997*, Orlando, FL, 1997.

[18] Letellier, A., Bung, H., Galon, P., and Berthillier, M., "Bird Impact on Fan Blade Analysis Using Smooth Particle Hydrodynamics Coupled with Finite Elements," *Structures Under Extreme Loading Conditions*, Vol. 351, ASME Pressure Vessels and Piping Division, Orlando Etats-unis, 1997, pp. 191–195.

[19] Audic, S., Berthillier, M., Bonini, J., Bung, H., and Combescure, A., "Prediction of Bird Impact in Hollow Fan Blades," AIAA Paper 2000-3201, July 2000.

[20] Guan, Y. P., Chen, W., and Huang, Z. Y., "Sliced Model for Bird Impacting Blades," *Journal of Nanjing University of Aeronautics and Astronautics*, Vol. 36, No. 6, 2004, pp. 784–786.

[21] Jones, N., and Wierzbicki, T., *Structural Crashworthiness and Failure*, Elsevier Science Publishers, London, 1993.

[22] Stoll, F., and Brockman, R. A., "Finite Element Simulation of High-Speed Soft-Body Impacts," *Proceedings of the 1997 38th AIAA/ASME/ASCE/AHS/ASC Structures, Structual Dynamics and Materials Conference, Part 1*, AIAA, Reston, VA, 1997, pp. 334–344.

[23] Anghileri, M., and Bisagni, C., "Specific Problems Related to Simulation of a Bird Impact Against a Turbofan Inlet," *Proceedings of the International Crashworthiness Conference 2000 (ICRASH 2000)*, London, Sept. 2000, pp. 652–662.

[24] Airoldi, A., and Tagliapietra, D., "Bird Impact Simulation Against a Hybrid Composite and Metallic Vertical Stabilizer," AIAA Paper 2001-1390, 2001.

[25] Vignjevic, R., Hughes, K., and Taylor, E. A., "Finite Element Modelling of Failure of a Multi-Material Target due to High Velocity Space Debris Impacts," *Space Debris*, Vol. 2, No. 1, March 2002, pp. 41–50.

[26] Airoldi, A., and Cacchione, B., "Numerical Analyses of Bird Impact on Aircraft Structures Undergoing Large Deformations and Localized Failures," *International Conference on Impact Loading of Lightweight Structures*, edited by M. Alves and N. Jones, *WIT Transactions on Engineering Sciences*, Vol. 49, 2005, pp. 1–18.

[27] Langrand, B., Bayart, A. S., Chauveau, Y., and Deletombe, E., "Assessment of Multi-Physics FE Methods for Bird Strike Modelling—Application to a Metallic Riveted Airframe," *International Journal of Crashworthiness*, Vol. 7, No. 4, 2002, pp. 415–428.

[28] Anghileri, M., Luigi, M. L. C., and Valerio, M., "Bird Strike: Approaches to the Analysis of Impacts with Penetration," *International Conference on Impact Loading of Lightweight Structures*, edited by M. Alves and N. Jones, *WIT Transactions on Engineering Sciences*, Vol. 49, 2005, pp. 63–74.

[29] Feng, Y. T., Han, K., and Owen, D. R. J., "Discrete Element Simulation of the Dynamics of High Energy Planetary Ball Milling Processes,"

Materials Science and Engineering. A, Structural Materials: Properties, Microstructure and Processing, Vols. 375–377, July 2004, pp. 815–819.

[30] Han, K., Peric, D., and Owen, D. R. J., "A Combined Finite/Discrete Element Simulation of Shot Peening Processes—Part 2: Interaction Laws," *Engineering Computations*, Vol. 17, No. 6, 2000, pp. 680–702.

[31] Gordon, R. J., Eric, H. P., and Robert, A. S., "Incorporation of an SPH Option into the Epic Code for a Wide Range of High Velocity Impact Computations," *International Journal of Impact Engineering*, Vol. 14, Nos. 1–4, 1993, pp. 385–394.

[32] Baughn, T. V., and Graham, L. W., "Simulation of a Bird Strike Impact on Aircraft Canopy Material," *Journal of Aircraft*, Vol. 25, No. 7, 1988, pp. 659–664.

[33] Brockman, R. A., and Held, T. W., "Explicit Finite Element Method for Transparency Impact Analysis," University of Dayton Research Institute, WL-TR-91-3006, Dayton, OH, 1991.

[34] Bouchard, M. P., and Davisson, J. C., "Advanced Transparency Development for USAF Aircraft," *34th AIAA/ASME/ASCE/AHS/ASC Structures, Structural Dynamics and Materials Conference, Part 2*, 1993, pp. 800–809.

[35] McCarthy, M. A., Xiao, J. R., McCarthy, C. T., Kamoulakos, A., Ramos, J., Gallard, J. P., and Melito, V., "Modelling of Bird Strike on an Aircraft Wing Leading Edge Made from Fibre Metal Laminates—Part 2: Modeling of Impact with SPH Bird Model," *Applied Composite Materials*, Vol. 11, No. 5, Sept. 2004, pp. 317–340.

[36] Rueda, F., Beltran, F., Maderuelo, C., and Climent, H., "Bird Strike Analysis of the Wing Slats of EF-2000," *Structures Under Shock and Impact 7*, Vol. 11, WIT Press, Southampton, U.K., 2002, pp. 189–198.

[37] Kari, S., Gabrys, J., and Lincks, D., "Bird Strike Analysis of Radome and Wing Leading Edge Using LS-DYNA," *ASME Pressure Vessels and Piping Division*, Vol. 414, Part 1, 2000, pp. 87–102.

[38] Bedrich, L., and Mertl, V., "Bird Impact Resistance of the Small Transport Aircraft," *Proceedings of the 20th Congress of the International Council of the Aeronautical Sciences (ICAS 96)*, Sorrento, Italy, Sept. 1996, pp. 175–182.

[39] Reddy, J. N., "A Finite Element Solution of Nonlinear PDE's in the Hydrodynamics of Hypervelocity Impact," *Advances in Computer Methods for Partial Differential Equations*, edited by R. Vichnevetsky, Rutgers University, Piscataway, NJ, 1975, pp. 220–224.

[40] Perzyna, P., "Fundamental Problems in Viscoplasticity," *Advances in Applied Mechanics*, Vol. 9, 1966, pp. 243–377.

[41] Willows, M., and Driffill, B., GARTEUR (Group for Aeronautical Research and Technology in EURope) Bird Strike Group, Round robin work package: Rigid wall phase 1 and task 1, DERA Farnborough, Building A7, Room 2008, Hants GU14 OLX, 1999.

[42] Seamans, T. W., Hamershock, D. W., and Bernhardt, G. E., "Determination of Body Density for 12 Bird Species," *Ibis*, Vol. 137, No. 3, 1995, pp. 424–428.